Nanoscale Research Letters
a SpringerOpen Journal

NANO EXPRESS

Open Access

Delayed crystallization of ultrathin Gd$_2$O$_3$ layers on Si(111) observed by *in situ* X-ray diffraction

Michael Hanke[*], Vladimir M Kaganer, Oliver Bierwagen, Michael Niehle and Achim Trampert

Abstract

We studied the early stages of Gd$_2$O$_3$ epitaxy on Si(111) in real time by synchrotron-based, high-resolution X-ray diffraction and by reflection high-energy electron diffraction. A comparison between model calculations and the measured X-ray scattering, and the change of reflection high-energy electron diffraction patterns both indicate that the growth begins without forming a three-dimensional crystalline film. The cubic bixbyite structure of Gd$_2$O$_3$ appears only after a few monolayers of deposition.

Background

Binary rare-earth metal oxides became increasingly important as gate dielectrics in metal oxide semiconductor field-effect transistor technology [1,2] and as catalysts. The application of these oxides as gate dielectrics is based on their high dielectric constants [3], large bandgaps [4], high thermal stability of their interfaces to silicon [5], and large band offsets with silicon. Gd$_2$O$_3$ is a promising candidate among the lanthanide oxides due to its close lattice match to silicon ($a_{Gd_2O_3} = 10.812 Å$; $2a_{si} = 10.862$ Å). Epitaxial growth of Gd$_2$O$_3$ has been demonstrated for a variety of substrates, including GaN [1], Si [6], and SiC [7] by atomic layer deposition [8] and molecular beam epitaxy (MBE) [9].

Here, we present an MBE growth study of Gd$_2$O$_3$ on Si(111), applying synchrotron-based X-ray diffraction with particular focus on the formation of the very first crystalline layers. These measurements were done during sample growth *in situ*, in a continuous way without any growth interruption.

Methods

Molecular beam epitaxy

All samples were grown in a dedicated MBE chamber under ultrahigh vacuum (UHV) conditions. The 2 × 2-cm^2 Si(111) substrates were prepared by a 10-min dilute (5%) HF treatment, to remove the thermal oxide, followed by a 10-min H$_2$O rinse. Next, they were loaded into the MBE system, degased at 300°C in the load lock for 20 min, and annealed in the growth chamber under UHV at 720°C (measured using a thermocouple between heater and substrate) for 60 min to prepare a (7 × 7) reconstructed Si(111) surface. The sample temperature was subsequently ramped to the growth temperature of 700 C. During the growth, Gd$_2$O$_3$ powder (99.999%) was evaporated from a special effusion cell (TUBO), which allows for cell temperatures in excess of 2,000°C [10]. Temperature and flux from this cell can be adjusted more accurately than with conventional e-beam evaporators. Throughout the experiment, the cell temperature was kept constant at 1,650°C (thermocouple temperature; the actual temperature of the source material is higher), resulting in a growth rate of 0.13 Å/min. Molecular oxygen at 10^{-7} mbar was added 30 s prior to the growth sequence and throughout the entire layer deposition (OB, unpublished work).

X-ray diffraction

The X-ray scattering experiments were performed at the dedicated beamline U125/2-KMC at the synchrotron BESSY II (Helmholtz-Zentrum Berlin HZB, Berlin, Germany). This experimental setup [11] combines the MBE system described above with the ability to perform high-resolution X-ray diffraction, which enables unique *in situ* growth studies. The primary X-ray beam with a size of 500 × 500 μm^2 enters and exits the growth chamber via X-ray transparent Be windows, whereas the scattered intensity can be probed in an angular range of 0° to 120° in-plane and 0° to 50° out-of-plane. Both the sample and the detector can be precisely moved during the

* Correspondence: hanke@pdi-berlin.de
Paul-Drude-Institut für Festkörperelektronik, Hausvogteiplatz 5-7, Berlin, D-10117, Germany

growth to probe scattered intensity in a wide range of reciprocal space. An X-ray energy E of 12 keV, selected by a Si(111) double crystal monochromator ($\Delta E/E = 10^{-4}$), is chosen as a compromise between the accessible area in reciprocal space and primary intensity. Throughout the experiment, the incidence angle was kept constant at $\alpha_i = 0.2°$.

Results and discussion

We index the reflections in surface (hexagonal) coordinates, marked with $(HKL)_{hex}$, instead of using bulk indices, denoted by $(HKL)_{cub}$ [12]. Referring to the symmetry of the $Si(111)_{cub}$ substrates, we define the surface unit cell by vectors **a**, **b**, and **c** with lengths $a = b = 3.84$ Å, $c = 9.405$ Å and $\alpha = \beta = 90°$, $\gamma = 120°$. For example, the $Si(022)_{cub}$ bulk reflection refers to $(104)_{hex}$ in surface coordinates.

Post-growth X-ray diffraction

Figure 1a shows a post-growth in-plane intensity distribution of a 13-monolayer (ML, 1 ML = 3.12 Å)-thick Gd_2O_3 layer on Si(111) measured by *in situ* X-ray diffraction. All reflections are labeled in the sketch (Figure 1b) which also addresses their different origin. There are basically three types of reflections: intense substrate peaks (red squares), layer reflections (blue circles), and intensity tails from crystal truncation rods (CTRs, green triangles), which are forbidden reflections for bulk Si. This diffraction pattern corresponds to the cubic bixbyite structure (space group 206) of Gd_2O_3 with single orientation, in agreement with previous studies, which

found an A-B twinning relation for $Gd_2O_3/Si(111)$ heteroepitaxy [13]. Thus, the layer is 180° rotated with respect to the underlying substrate, referring to the Si-CaF_2-type interface with the silicon atoms directly bonded to calcium [14].

In-situ X-ray studies during growth

To study the epitaxial growth of Gd_2O_3 on Si(111) *in situ*, we probed the evolution of the out-of-plane scattering by measuring three different CTRs, whose positions are indicated by green triangles in Figure 1b. Figure 2 shows measured (a, b) and calculated (c, d) intensity distributions along the CTRs $(10L)_{hex}$ and $(20L)_{hex}$ for layer thicknesses of up to 14 ML. The third measured CTR, $(1\bar{1}L)_{hex}$, is not shown. Since the growth was continuous without any interruption, the thickness changes during an individual CTR scan by approximately 0.6 ML. The depicted scan range in L covers two silicon peaks, namely $Si(1\bar{1}1)_{cub}$ and $Si(022)_{cub}$ at the CTR $(10L)_{hex}$, as well as $Si(\bar{2}22)_{cub}$ and $Si(\bar{1}33)_{cub}$ at the CTR $(20L)_{hex}$. Due to the A-B twinning relation to the substrate, the layer peaks do not coincide with those of the substrate. Gd_2O_3 in its bixbyite structure exhibits a lattice parameter a of 10.812 Å (1 ML in [111] direction refers to $a/2\sqrt{3} = 3.12\,Å$), which nearly equals the substrate value. The resulting lattice mismatch is as small as 0.4%. Such a type of layer (closely lattice-matched and A-B-twinned with respect to the substrate) will excite reflections shifted from
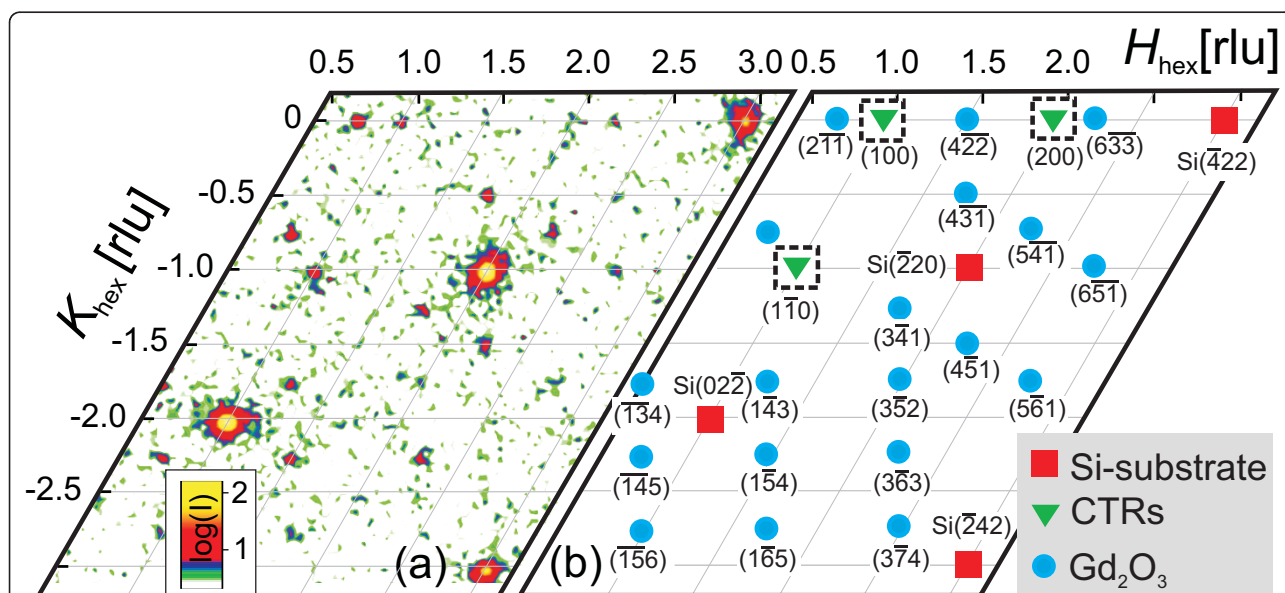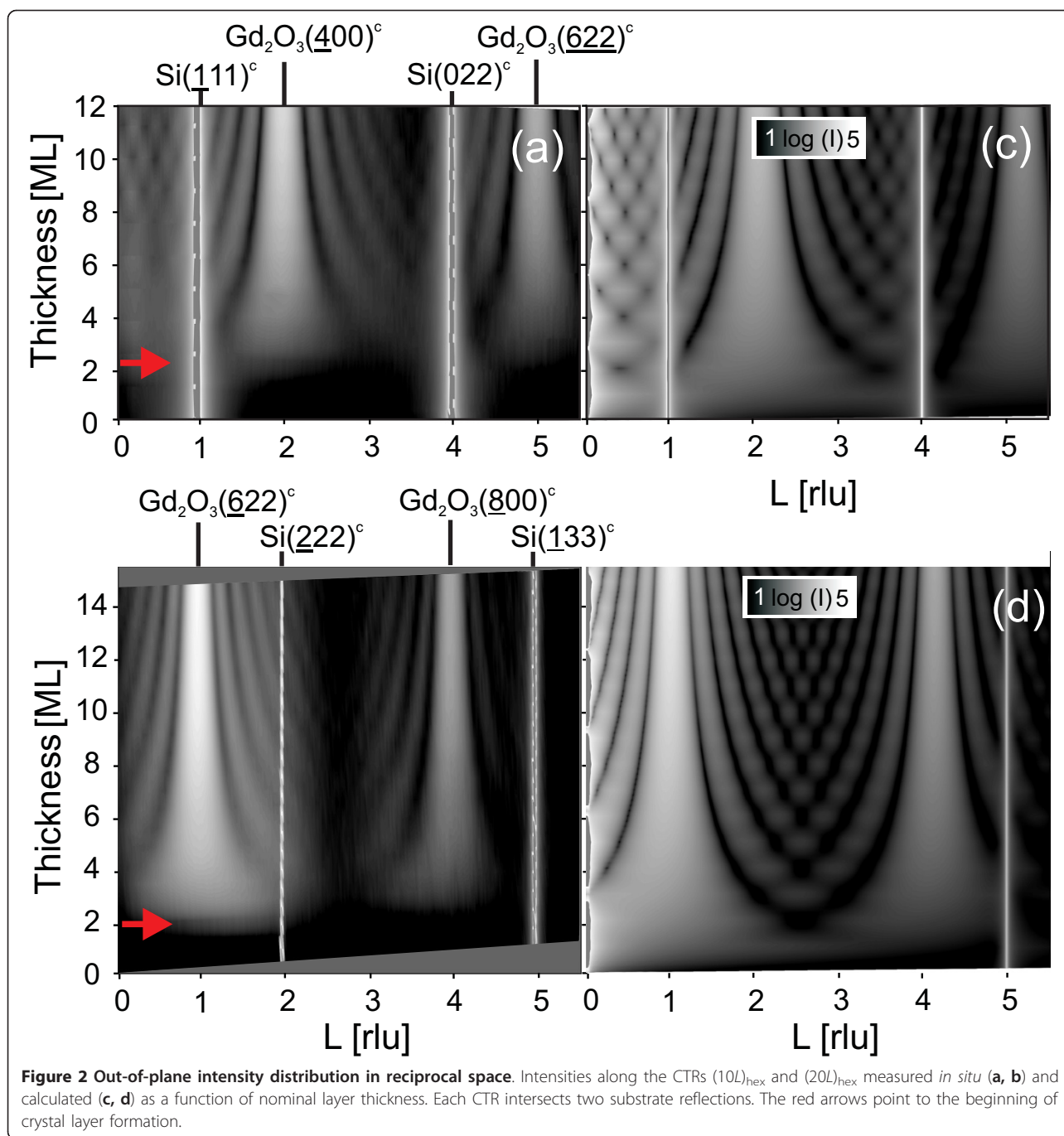

Figure 1 In-plane intensity distribution in reciprocal space. (**a**) Measured and (**b**) schematic in-plane intensity distribution showing the Gd_2O_3 bixbyite (blue circles) and substrate (red squares) reflections, and the tails of the CTRs $(10L)_{hex}$, $(20L)_{hex}$, and $(1\bar{1}L)_{hex}$ (green triangles).

Figure 2 Out-of-plane intensity distribution in reciprocal space. Intensities along the CTRs $(10L)_{hex}$ and $(20L)_{hex}$ measured *in situ* (**a, b**) and calculated (**c, d**) as a function of nominal layer thickness. Each CTR intersects two substrate reflections. The red arrows point to the beginning of crystal layer formation.

substrate contributions by $L = \pm 1$ as shown in Figure 2. The onset of these layer reflections sensitively probes the appearance of a three-dimensional crystalline Gd_2O_3 lattice.

Scattering calculations

For comparison, the CTR intensities were calculated using the structure model shown in Figure 3a. The semi-infinite silicon substrate and a finite number of the oxide layers, in a twinned orientation of the ABCABC packing with respect to the substrate, were included in the calculation. The intensity calculations were performed in the distorted wave Born approximation [15] since the incidence angle is close to the critical angle. A non-integer deposition was calculated as a sum of scattering amplitudes of two films, with the integer numbers of monolayers smaller and larger than the actual deposition, taken in the appropriate proportion. The time-dependent layer thickness was
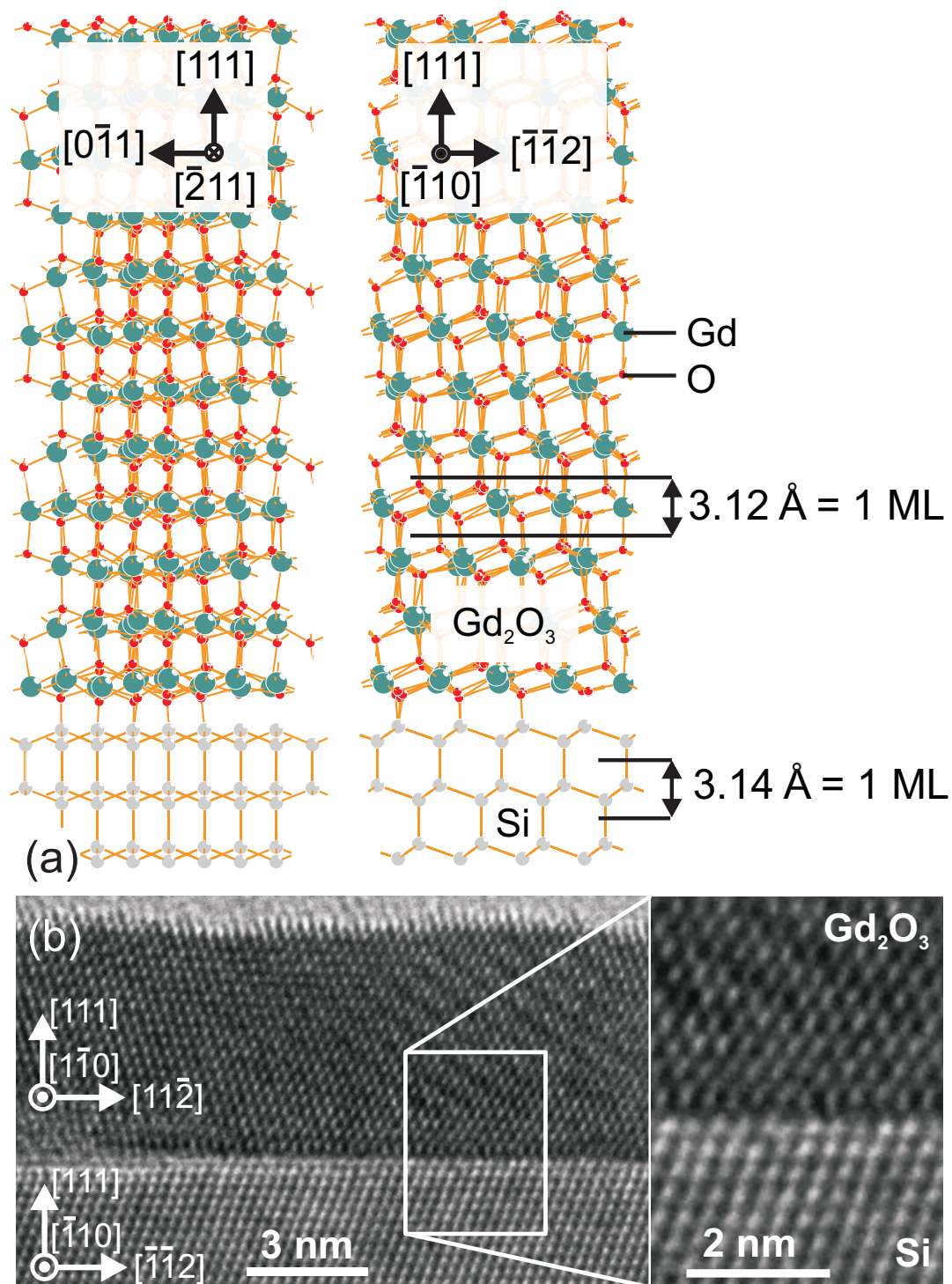
Figure 3 Real-space structure of Gd_2O_3 on Si(111). (**a**) Structure model shown in two different azimuths $[0\bar{1}1]$ and $[\bar{1}\bar{1}2]$. (**b**) A transmission electron micrograph of the layer and the interface region.

determined from the current growth time. The growth rate was obtained by dividing the total film thickness, determined from a post-growth CTR measurement, by the total growth time.

Layer formation at the interface

The measured (Figure 2a, b) and calculated (Figure 2c, d) intensity distributions agree for a layer thickness larger than about 3 ML (indicated by red arrows in the

figure). Layer peaks become stronger and are subsequently accompanied by thickness fringes whose separation in *L* shrinks with increasing thickness. However, in contrast to the calculations, which contain a fingerprint of a three-dimensional crystalline Gd_2O_3 lattice already from the first monolayer on, there is no experimental evidence for a crystalline layer below the deposition of 2 to 3 ML. For a more detailed analysis, Figure 4

compares a selection of measured and calculated CTRs at different deposition thicknesses. The measured CTRs do not show an indication of the crystalline film for the deposition less than 2 ML, while the intensity changes due to the film are visible on the calculated CTRs from the very beginning of the growth. We cannot exclude an in-plane ordering in separate layers without any registry among one another. At depositions between 2 and
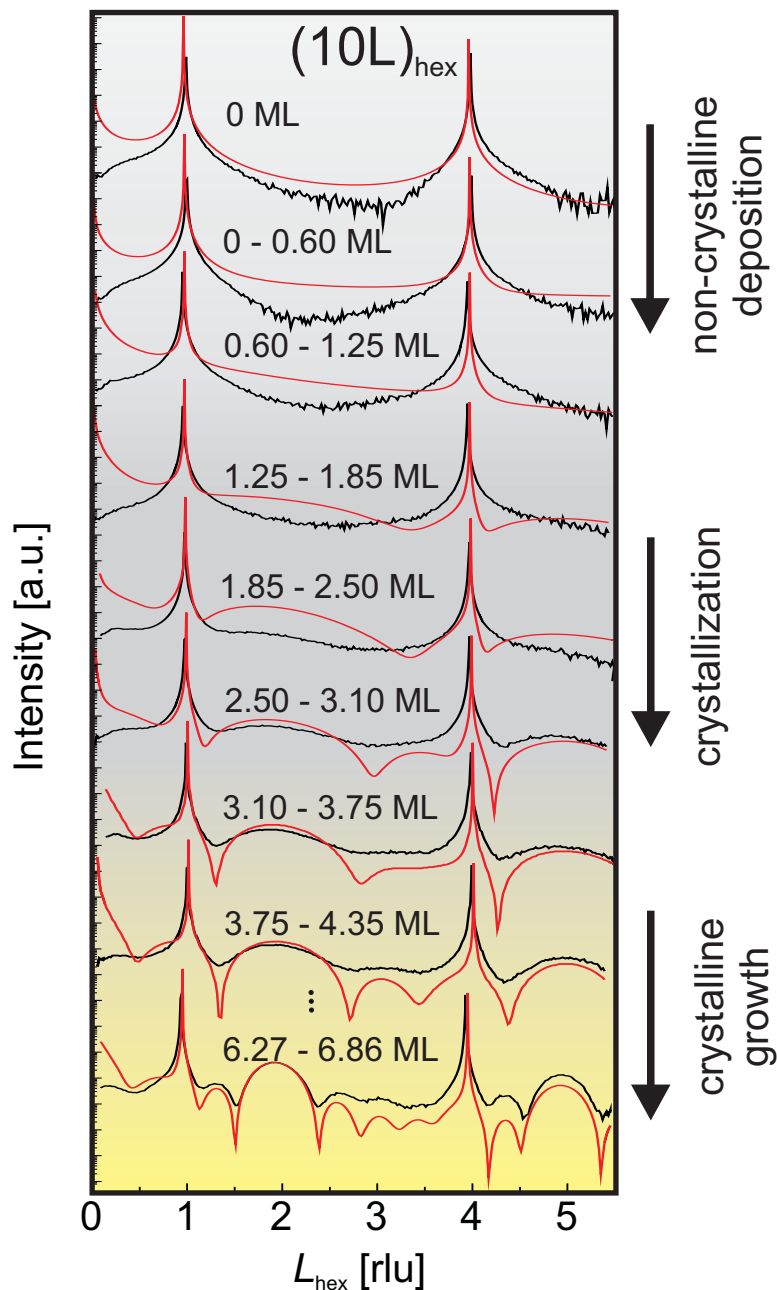

Figure 4 Comparison between measured and simulated CTRs. One-dimensional intensity profiles along the CTR (10*L*)hex as measured (black curves) and calculated (red). The given values refer to nominally deposited layer thickness. In the beginning, the experimental profile does not change (gray), followed by a crystallization process (dark gray) which finally ends up with crystalline growth (yellow).

about 4 ML, the measured curves become more and more close to the calculated ones, showing that the crystalline order develops in the film. For the film thickness larger than 4 ML, a crystalline film grows, and the thickness determined from the fringes on the CTRs agrees with the nominally deposited film thickness. This agreement proves that the sticking coefficient is constant for the entire growth starting from the layer-substrate interface - consistent with a constant deposition rate.

Atomic force microscopy of the pure Si(111) substrate (not shown) yields a mean terrace size of 600 nm, which does not change after the deposition of 1 and 2 ML of Gd_2O_3. The roughness of 0.46 nm is preserved during growth. Post-growth X-ray reflectivity measurements prove the nominal layer thickness with an RMS roughness of less than 1 ML.

The evolution of the reflection high-energy electron diffraction (RHEED) pattern (not shown) during the first MLs is consistent with the 'delayed crystallization' scenario: During deposition of the first ML, the 2D streaky RHEED pattern from the Si(111) surface disappeared completely and transformed into a diffuse RHEED pattern with almost vanishing specular spot intensity - indicative of the lack of crystal order [13]. The specular spot intensity recovered after the deposition of (3 to 5 ML) together with the onset of pronounced RHEED oscillations.

For the final film, the fringes of CTRs (sensitive to crystalline film thickness only) and the X-ray reflectivity fringes (sensitive to total film thickness irrespective of crystalline order) correspond to the same thickness. Therefore, the crystalline order developed over the whole film thickness, without leaving a noncrystalline initial layer at the interface. This conclusion is in agreement with cross-sectional transmission electron micrographs in Figure 3b which demonstrates a pseudomorphic film and an atomically flat layer-substrate interface.

Conclusions

We have performed a synchrotron-based *in situ* X-ray diffraction study during the epitaxial growth of Gd_2O_3 on Si(111). By comparing measured crystal truncation rods to X-ray scattering calculations, we found that the crystallization into three-dimensional cubic bixbyite structure was delayed: it started at a layer thickness of about 2 ML and proceeded up to 4 ML.

Abbreviations

CTR: crystal truncation rod; MBE: molecular beam epitaxy; ML: monolayer; RHEED: reflection high-energy electron diffraction; TEM: transmission electron microscopy; UHV: ultrahigh vacuum.

References

1. Chang WH, Lee CH, Chang YC, Chang P, Huang ML, Lee YJ, Hsu CH, Hong JM, Tsai CC, Kwo JR, Hong M: **Nanometer-thick single-crystal hexagonal Gd-2₃ on GaN for advanced complementary metal-oxide-semiconductor technology.** *Adv Mater* 2009, **21**:4970.
2. Mahajan SV, Dickerson JH: **Dielectric properties of colloidal Gd-2₃ nanocrystal films fabricated via electrophoretic deposition.** *Appl Phys Lett* 2010, **96**:113105.
3. Kwo J, Hong M, Kortan AR, Queeney KT, Chabal YJ, Mannaerts JP, Boone T, Krajewski JJ, Sergent AM, Rosamilia JM: **High epsilon gate dielectrics Gd-2₃ and Y-₂₃ for silicon.** *Appl Phys Lett* 2000, **77**:130.
4. Badylevich M, Shamuilia S, Afanas'ev VV, Laha A, Osten JH, Fissel A: **Investigation of the electronic structure at interfaces of crystalline and amorphous Gd-₂₃ thin layers with silicon substrates of different orientations.** *Appl Phys Lett* 2007, **90**:252101.
5. Hubbard KJ, Schlom DG: **Thermodynamic stability of binary oxides in contact with silicon.** *J Mater Res* 1996, **11**:2757.
6. Wang JX, Laha A, Fissel A, Schwendt D, Dargis R, Watahiki T, Shayduk R, Braun W, Liu TM, Osten HJ: **Crystal structure and strain state of molecular beam epitaxial grown Gd₂₃ on Si(111) substrates: a diffraction study.** *Semicond Sci Technol* 2009, **24**:045021.
7. Fissel A, Czernohorsky M, Osten HJ: **Growth and characterization of crystalline gadolinium oxide on silicon carbide for high-K application.** *Superlatt Microstruct* 2006, **40**:551.
8. Niinistö J, Petrova N, Putkonen M, Niinistö L, Arstila K, Sajavaara T: **Gadolinium oxide thin films by atomic layer deposition.** *Jour Cryst Growth* 2005, **285**:191.
9. Lin TD, Hang MC, Hsu CH, Kwo J, Hong M: **MBE grown high-quality Gd-2₃/Si(111) hetero-structure.** *Jour Cryst Growth* 2007, **301**:386.
10. Watahiki T, Jenichen B, Shayduk R, Tinkham BP, Braun W, Riechert H: **Structure analysis of epitaxial Gd-2₃/Si(001) for high-k gate dielectric applications.** *Jour Cryst Growth* 2009, **311**:2179.
11. Jenichen B, Braun W, Kaganer V, Shtukenberg A, Däweritz L, Schulz C, Ploog K, Erko A: **Combined molecular beam epitaxy and diffractometer system for in situ x-ray studies of crystal growth.** *Rev Sci Instrum* 2003, **74**:1267.
12. Grübel G, Huang KG, Gibbs D, Zehner DM, Sandy AR, Mochrie SGJ: **Reconstruction of the Pt(111) surface - x-ray scattering measurements.** *Phys Rev B* 1993, **48**:18119.
13. Fissel A, Kühne D, Bugiel E, Osten HJ: **Cooperative solid-vapor-phase epitaxy: an approach for fabrication of single-crystalline insulator/Si/insulator nanostructures.** *Appl Phys Lett* 2006, **88**:153105.
14. Schroeder BR, Meng S, Bostwick A, Olmstead MA: **Epitaxial growth of laminar crystalline silicon on CaF-2.** *Appl Phys Lett* 2000, **77**:1289.
15. Kaganer VM: **Crystal truncation rods in kinematical and dynamical x-ray diffraction theories.** *Phys Rev B* 2007, **75**:245425.